Supplement of Atmos. Chem. Phys., 20, 11451–11467, 2020
https://doi.org/10.5194/acp-20-11451-2020-supplement

Atmospheric Chemistry and Physics
Open Access
EGU

Supplement of

Formation and sink of glyoxal and methylglyoxal in a polluted subtropical environment: observation-based photochemical analysis and impact evaluation

Zhenhao Ling et al.

Correspondence to: Zhe Wang (z.wang@ust.hk) and Xuemei Wang (eciwxm@jnu.edu.cn)

Section S1 The supplementary Tables and Figures in the manuscript.

Table S1. Model scenarios used for gas-phase Mgly.

Model scenarios	Description
INITIAL	Default MCMv3.2, without considering the reversible and irreversible uptake of Mgly and the gas-particle partitioning of other oxidation products.
Scenario M1	As INITIAL, and considers Mgly partitions into the liquid-phase, without considering the monomers pool 1 and oligomers pool 2.
Scenario M2	As Scenario M1, and considers surface uptake by aerosols of Mgly with the uptake coefficient of 2.6×10^{-4}(Pye et al., 2017).

Table S2. The selected NMHC species for the input of PBM-MCM model

No.	Compound	No.	Compound
1	Ethane	23	1-Butene
2	Propane	24	cis-2-Butene
3	i-Butane	25	1-Pentene
4	n-Butane	26	trans-2-Pentene
5	i-Pentane	27	Isoprene
6	n-Pentane	28	cis-2-Pentene
7	2,2-Dimethylbutane	29	1-Hexene
8	2,3-Dimetylbutane	30	1,3-Butadiene
9	2-Methylpentane	31	Benzene
10	3-Methylpentane	32	Toluene
11	n-Hexane	33	Ethylbenzene
12	2-Methylhexane	34	m/p-Xylene
13	Cyclohexane	35	o-Xylene
14	3-Methylhexane	36	Styrene
15	n-Heptane	37	i-Propylbenzene
16	n-Octane	38	n-Propylbenzene
17	n-Nonane	39	m-Ethyltoluene
18	n-Decane	40	p-Ethyltoluene
19	Ethene	41	1,3,5-Trimethylbenzene
20	Propene	42	o-Ethyltoluene
21	Ethyne	43	1,2,4-Trimethylbenzene
22	trans-2-Butene	44	1,2,3-Trimethylbenzene

Table S3. The mean measured OH and HO_2 concentrations in the previous studies and our model results (in molecule·cm^{-3})

Location	season	OH (× 10^6)	HO_2 (× 10^8)	year	Reference
PRD, China	Summer	15	-	2006	(Hofzumahaus et al., 2009)
Shanghai, China		10.2	-	2013	(Nan et al., 2017)
north-western Greece		8	4.7	1997	(Creasey et al., 2001)
PRD, China	Autumn	4.5	3.0	2014	(Tan et al., 2019)
Tokyo, Japan	Winter	1.5	-	2004	(Kanaya et al., 2007)
New York, America		1.4	-	2004	(Ren et al., 2006)
Beijing, China		1.5	0.3	2017	(Ma et al., 2019)
PRD, China		1.6	0.3	2017	This study

Table S4. Estimated uncertainties of model reaction rate constant and input parameters.

Input parameter	Uncertainty factor
j[a]	×1.1
τD	×2
T	×1.005
P	×1.005
OH	×1.2
H_2	×1.2
CO	×1.05
NO	×1.07
NO_2	×1.13
O_3	×1.05
H_2O	×1.1
HONO	×1.1
CH_4	×1.04
Ethane [b]	+0.2 ppb
Ethene [b]	+0.7 ppb
Ethyne [b]	+1.2 ppb
C_3-C_{10} NMHCs	×1.2
K_i [c]	×1.3

[a] The errors of the measured photolysis frequencies are assumed to be correlated since they were derived from the same measurement of the solar actinic flux. [b] Campaign averaged values were applied for ethane, ethene, and ethyne, so that the standard deviation of the canister samples were propagated as uncertainties rather than the measurement accuracy. [c] All the reaction constants of non-photolytic reactions in MCM v3.2 are estimated to have 30% accuracy (1σ)(Li et al., 2014; Lu et al., 2012).

Table S5. Linear regression coefficients and relative contributions of primary, secondary, and background sources of Gly and Mgly.

	Linear regression coefficients			Source Contribution			
	β_0	β_1	β_2	Background	Primary	Secondary	R
Gly	0.001	0.066	0.042	0.40%	3.46%	96.14%	0.77
Mgly	0.002	0.108	0.081	0.05%	3.51%	96.44%	0.75

To estimate the contributions of primary sources to measured Gly and Mgly, a correlation-based source apportionment method suggested by previous studies was used, as described by equation 1 (Friedfeld et al., 2002; Yuan et al., 2013) .

$$[dicarbonyls] = \beta_0 + \beta_1[C_2H_2] + \beta_2[O_3] \quad (1)$$

where β_0, β_1, and β_2 are the coefficients derived from the linear regression analysis. For every unit increase in C_2H_2 concentration there is a β_1 unit increase in dicarbonyls. Similarly, for every unit increase in O_3 concentration there is a β_2 unit increase in dicarbonyls. β_0 can be considered the background dicarbonyls level (in units of ppbv). Relative contributions from primary emissions, secondary formation, and background dicarbonyls concentrations can be computed according to the tracer concentrations and corresponding β -values by the following equations:

$$P_{primary} = \frac{\beta_1[C_2H_2]i}{(\beta_0+\beta_1[C_2H_2]i+\beta_2[O_3]i)} \times 100\% \quad (2)$$

$$P_{secondary} = \frac{\beta_2[O_3]i}{(\beta_0+\beta_1[C_2H_2]i+\beta_2[O_3]i)} \times 100\% \quad (3)$$

$$P_{background} = \frac{\beta_0}{(\beta_0+\beta_1[C_2H_2]i+\beta_2[O_3]i)} \times 100\% \quad (4)$$

Table S6 the sensitivity test of physical processes

	Gly (ppbv)			Mgly (ppbv)		
time	INITIAL[a]	Dry depsition[b]	Duiltion[c]	INITIAL[a]	Dry deposition[b]	Dilution[c]
6:00	0.004	0.004	0.004	0.005	0.005	0.005
7:00	0.017	0.017	0.016	0.021	0.021	0.020
8:00	0.036	0.036	0.032	0.047	0.046	0.045
9:00	0.072	0.071	0.067	0.092	0.092	0.088
10:00	0.140	0.138	0.128	0.180	0.177	0.169
11:00	0.224	0.220	0.206	0.311	0.307	0.291
12:00	0.309	0.300	0.284	0.449	0.420	0.419
13:00	0.364	0.354	0.332	0.509	0.500	0.473
14:00	0.400	0.392	0.367	0.541	0.531	0.498
15:00	0.393	0.379	0.359	0.501	0.490	0.459
16:00	0.373	0.359	0.339	0.455	0.442	0.416
17:00	0.376	0.361	0.340	0.441	0.430	0.400
18:00	0.365	0.350	0.322	0.424	0.410	0.384
19:00	0.353	0.336	0.314	0.406	0.390	0.367

[a] Data modeled from the INITIAL scenario.

[b] Based on the INITIAL scenario, the dry deposition rate multiplied by two for Gly/Mgly modeled.

[c] Based on the INITIAL scenario, the dilution rate multiplied by two for Gly/Mgly modeled.

Table S7. Absolute and relative changes of Gly mixing ratio, and the contribution of differ aerosol sinks to total heterogeneous loss of Gly under different model simulations for the Heshan site. When the model scenario is changing from A to B, the absolute changes of Gly mixing ratio is calculated as $\triangle Gly = B - A$; the relative change in percentage is calculated as $\% = 100\times \triangle Gly / A$.

Scenario	Time period	Relative change in Gly
INITIAL → scenario 1	06-12	-1.70%
	13-19	-0.60%
	06-19	-1.20%
Scenario 1 → scenario 2	06-12	-1.40%
	13-19	-2.40%
	06-19	-1.90%
Scenario 2 → scenario 3	06-12	-17.3%
	13-19	-34.0%
	06-19	-25.7%
Scenario 3 → scenario 4	06-12	-55.0%
	13-19	-68.4%
	06-19	-61.7%
INITIAL → scenario 4	06-12	-65.0%
	13-19	-79.6%
	06-19	-72.3%

Table S8. Absolute and relative changes of Mgly mixing ratio, and the contribution of differ aerosol sinks to total heterogeneous loss of Mgly under different model simulations for the Heshan site. When the model scenario is changing from A to B, the absolute changes of Mgly mixing ratio is calculated as △Mgly = B − A; the relative change in percentage is calculated as % = 100× △Mgly / A.

scenario	Time period	Relative change in Mgly
INITIAL → scenario M1	06-12	-46.0%
	13-19	-36.7%
	06-19	-41.3%
Scenario M1 → scenario M2	06-12	-50.5%
	13-19	-60.9%
	06-19	-55.7%
INITIAL → scenario M2	06-12	-61.4%
	13-19	-82.6%
	06-19	-73.0%

Table S9. The relative contributions of different loss pathways of Gly and Mgly at nighttime

Loss pathyways	Gly	Mgly
NO_3,OH-reaction, %	2.44	3.56
dry deposition, %	1.04	0.74
dilution, %	1.92	1.60
heterogeneous [a], %		
Irreversible processes, %	57.9	55.9
Reversible processes, %	36.7	38.2

[a] Considered both irreversible and reversible parameterizations of the aerosol sinks (*i.e.*, scenario 4 and M2).

Table S10. Comparison of the results from this work and previous researches in PRD

	This study								Li Nan's study			
	Gly		Mgly		Gly		Mgly		Gly		Mgly	
	γ^a= 1×10^{-3}				γ = 2.9×10^{-3}				γ = 2.9×10^{-3}			
	SOA[b]	% [c]	SOA	%	SOA	%	SOA	%	SOA	%	SOA	%
m,p-Xylene	0.063	2.6%	0.081	3.3%	0.55 0.64[d]	8.0% 9.4%	0.56 0.81	8.2% 11.8%	0.20	2.2%	0.23	2.5%
o-Xylene	0.023	0.93 %	0.014	0.57%	0.18 0.19	2.6% 2.8%	0.09 0.13	1.3% 1.9%				
Toluene	0.079	3.2%	0.019	0.77%	0.63 0.77	9.2% 11%	0.13 0.19	1.9% 2.8%	0.16	1.8%	0.07	0.77%
SOA_{het}	0.28	11%	0.25	10%	2.1 2.5	31% 37%	2.0 2.4	29% 35%	2.33	26%	2.51	27%

[a] Uptake coefficients.
[b] Unit: μg/m^3.
[c] The contribution to the total SOA (i.e., SOA_{gp}+SOA_{het})
[d] Solely a surface uptake process for aerosol sink marked in red.

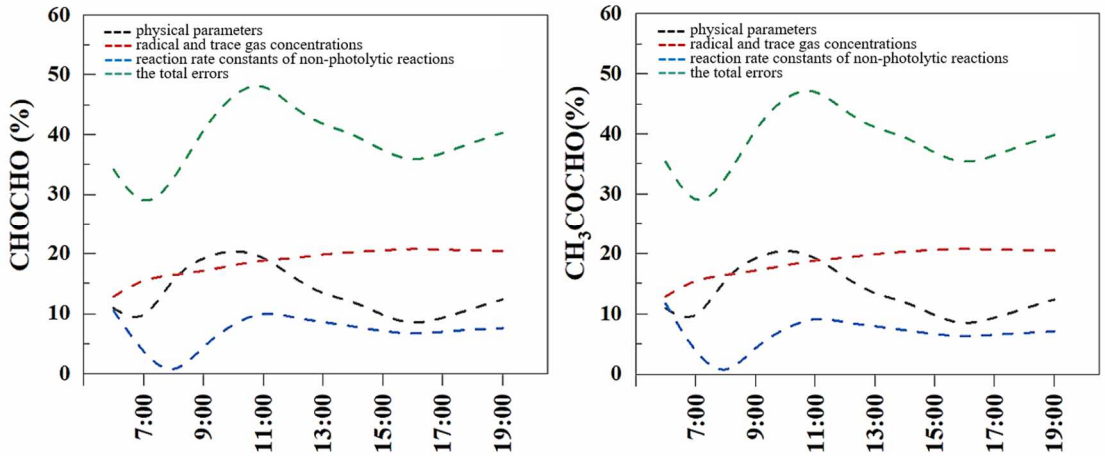

Figure S1. Mean diurnal variation of the uncertainty of the Gly and Mgly concentrations predicted by $MCM_v3.2$ model.

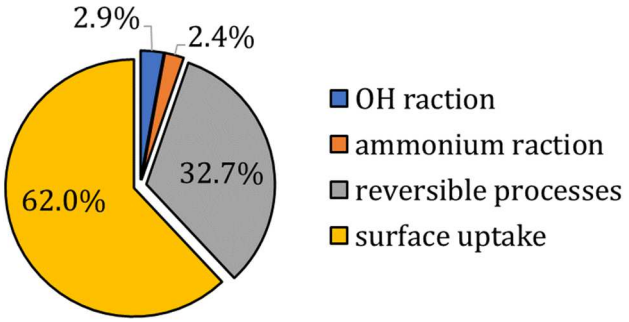

Figure S2. the contribution of differ aerosol sinks is calculated under the scenario 4.

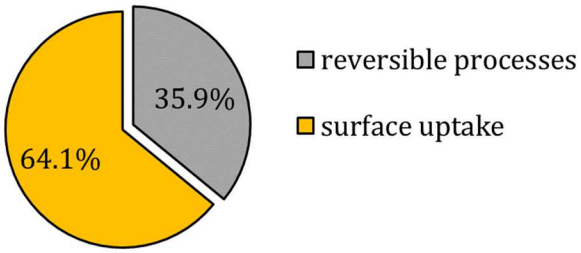

Figure S3. the contribution of differ aerosol sinks is calculated under the scenario M2.

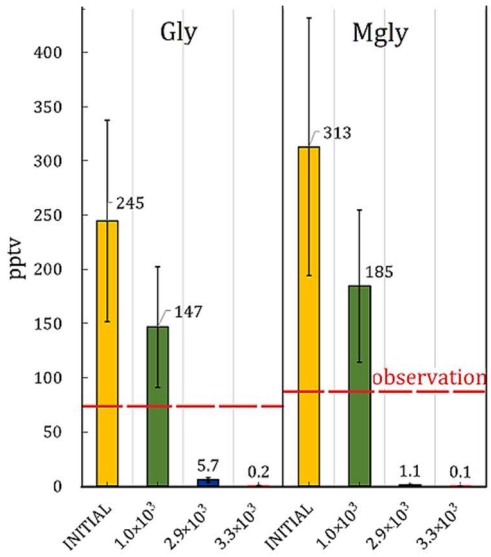

Figure S4. the daily average concentration of Gly and Mgly predicted from INITIAL and surface uptake scenarios (i.e., as INITIAL, and considers surface uptake by aerosols of Mgly and Mgly with the uptake coefficient of 1.0×10^3, 2.9×10^3, 3.3×10^3, respectively).

Section S2. The definition and configuration of each parameter used in equations 4-8

The reversible partitioning of Gly and Mgly on aerosols aqueous phase is usually described by the Henry's law equilibrium (Kampf et al., 2013) (Eq.4):

$$[Gly(Mgly)]_{liquid} = K_H \times [Gly(Mgly)]_{gas} \quad \text{(Eq.4)}$$

where $[Gly(Mgly)]_{liquid}$ and the $[Gly(Mgly)]_{gas}$ denote the concentration of Gly and Mgly in liquid-phase and gas-phase, respectively, whereas K_H (mol L^{-1} atm^{-1}) represents the Henry's law coefficient. Recently laboratorial studies had indicated that hydration of carbonyls function groups and salt-Gly interactions could have significant influences on the K_H value of Gly (Kampf et al., 2013; Waxman et al., 2015). Thus, an effective Henry's law coefficient expressed by Eq.5 was often used.

$$K_{H,effective} = \frac{K_{H,water}}{10^{(-0.24\min(12.0,(C_{as}+C_{an}))}} \quad \text{(Eq.5)}$$

where $K_{H,water}$ represents the henry's law constant of Gly observed for water, with value of 4.19×10^5 M atm^{-1} (Kampf et al., 2013). -0.24 is the "salting–in" constant of ammonium sulfate and nitrate (Kampf et al., 2013; Waxman et al., 2015). The concentrations of ammonium sulfate and nitrate are defined as C_{as}(M) and C_{an}(M), respectively. Furthermore, it was suggested that a low increase of $K_{H,effective}$ could be found at high concentrations of ammonium sulfate and nitrate (*i.e.,* 12 M) within the time scales of their experiments (*i.e.,* 60×10^3 s), while the equilibrium for Gly partitioning could be reached rapidly when the concentrations of ammonium sulfate and nitrate were lower (*i.e.,* < 12 M) (Kampf et al., 2013).

As variations were found for the value of $K_{H,effective}$ under different concentrations of ammonium sulfate and nitrate in previous studies (Erverns and Volkamer, 2010; Knote et al., 2014; Kampf et al., 2013), we calculated this vital parameter (*i.e.,* C_{as} + C_{an} for each hour in the present study. The C_{as} and C_{an} were calculated from the measured ammonium sulfate (or ammonium nitrate) concentrations (mol m^{-3}) divided by aerosol liquid water content (ALWC, kg m^{-3}), which were determined by the aerosol inorganics model (AIM-IV, http://www.aim.env.uea.ac.uk/aim/model4/model4a.php)

with inputs of the observed parameters (*e.g.*, ambient relative humidity, temperature, and the moles of each ion) at the Heshan site (Chang et al., 2019).

The reversible formation of monomer (*i.e.*, glyoxal, glyoxal monohydrate, and glyoxal dihydrate) and oligomers are considered with the two important reservoirs (*i.e.*, monomer and oligomer pools, represented as pool1 and pool2 in Knote et al. (2014)). The variations of the glyoxal monomer ([Gly_{p1}]) and oligomer concentrations ([Gly_{p2}]) with time can be represented based on Erverns and Volkamer, (2010), Kampf et al. (2013) and Knote et al. (2014), as follows:

$$\frac{d([Gly_{p1}])}{dt} = \frac{1}{\tau_1} \times (Gly_{p1,eq} - Gly_{p1}) \text{ (Eq.6)}$$

$$\frac{d([Gly_{p2}])}{dt} = \frac{1}{\tau_2} \times (Gly_{p2,eq} - Gly_{p2}) \text{ (Eq.7)}$$

$$\frac{Gly_{p2,eq}}{Gly_{p1,eq}} = K_{olig} \text{ (Eq.8)}$$

Where Gly_{p1} and Gly_{p2} were the current concentrations of Gly in monomers and oligomers pool, respectively. $Gly_{p1,eq}$ and $Gly_{p2,eq}$ were the concentrations in each pool at equilibrium, while τ_1 and τ_2 were the characteristic time scales to fill the monomer/oligomer pools, respectively.

Section 3. The validation of SOA simulation by the PBM-MCM model

As there were no direct SOA measurement data such as AMS data, we compared the model simulated SOA concentrations with those calculated by different methods and parameters, to evaluate the performance of SOA simulation.

First, the EC (elemental carbon)-tracer method was used here to estimate the concentration of SOA in the present study, according to the equations 1-2 (Duan et al., 2005):

$$SOC = OC_{tot} - EC \times (OC / EC)_{min} \quad (1)$$

$$SOA = S0C \times Coef_{SOA/SOC} \quad (2)$$

where *SOC* represents the secondary organic carbon; OC_{tot} represents the measured concentration of total organic carbon; $(OC/EC)_{min}$ is the emission ratio of primary OC (organic carbon) and EC (elemental carbon) from the sources, and can be represented by the minimum *OC/EC* ratio measured. Based on the $(OC/EC)_{min}$ value which was derived from the hourly observation data during the simulation period (i.e., January 07-08) using the minimum R squared (MRS) method and the hourly measured OC and EC concentrations (details in Chang et al., 2019), as well as the ratio of $Coef_{SOA/SOC}$ (Bae et al., 2006; Turpin and Lim, 2001), the mean concentration of SOA calculated by the EC-tracer method was 2.82 μg/m^3, about 1.2 times the model simulated SOA concentration in the present study (2.47 μg/m^3), suggesting that the PBM-MCM model provided a reasonable performance on the simulation of the magnitude of SOA, though uncertainties were frequently observed from the SOA concentrations calculated by the EC-tracer method.

Second, we also conducted the comparison between measurement and simulation on other secondary products, including acetic acid, formic acid and pyruvic acid, which have been recognized as key SOA species, to further evaluate the model performance (Figure 1). It was found that the simulated concentrations of acetic acid, formic acid and pyruvic acid were close to those observed at the Heshan site, accounting for ~80%, 70% and 88% of observed values for acetic acid, formic acid and pyruvic acid, respectively. The results confirmed that secondary formation was the dominant source of above species at the Heshan site, and suggested that the PBM-MCM model could

provide robust performance on simulating the abundance of above secondary species. The deviations between simulated and observed concentrations may be related to the lack of consideration of primary emissions and/or other production pathways of above species in the model. Nevertheless, the above comparisons confirmed that the PBM-MCM model in this study indeed provided an appropriate description on the formation of SOA and other secondary organic products.

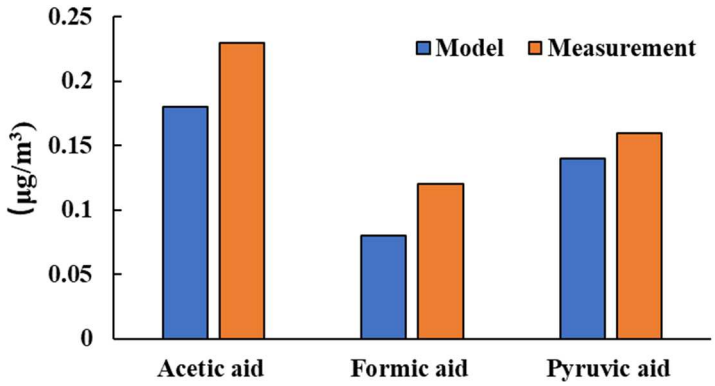

Fig S5. The concentrations of acetic acid, formic acid and pyruvic acid in filter samples

References

Bae, M. S., Demerjian, K. L, and Schwab, J. J.: Seasonal estimation of organic mass to organic carbon in PM2.5 at rural and urban locations in New York state, Atmos. Environ., 40, 7467-7479, 2006.

Chang, D., Wang, Z., Guo, J., Li, T., Liang, Y. H., Kang, L. Y., Xia, M., Wang, Y., Yu, C., Yun, H., Yue, D. L., and Wang, T.: Characterization of organic aerosols and their precursors in southern China during a severe haze episode in January 2017, Sci. Total Environ., 691, 101-111, 2019.

Creasey, D. J., Heard, D. E., Lee, J. D.: OH and HO_2 measurements in a forested region of north-western Greece, Atmos. Environ., 35, 4713-4724, 2001.

Duan, F., He, K., Ma, Y., Jia, Y., Yang, F., Lei, Y., and Okuta, T.: Characteristics of carbonaceous aerosols in Beijing, China, Chemosphere, 603, 355-364, 2005.

Ervens, B., and Volkamer, R.: Glyoxal processing by aerosol multiphase chemistry: towards a kinetic modeling framework of secondary organic aerosol formation in aqueous particles, Atmos. Chem. Phys., 1017, 8219-8244, 2010.

Friedfeld, S., Fraser, M., Ensor, K., Tribble, S., Rehle, D., Leleux, D., and Tittel, F.: Statistical analysis of primary and secondary atmospheric formaldehyde, Atmos. Environ., 36, 4767-4775, 2002.

Hofzumahaus, A., Rohrer, F., Lu, K. D., Bohn, B., Brauers, T., Chang, C.-C., Fuchs, H., Holland, F., Kita, K., Kondo, Y., Li, X., Lou, S.R., Shao, M., Zeng, L., Wahner, A., and Zhang, Y. H.: Amplified trace gas removal in the troposphere, Science, 324, 1702-1704, 2009.

Kampf, C. J., Waxman, E. M., Slowik, J. G., Dommen, J., Pfaffenberger, L., Praplan, A. P., André S. H., Baltensperger, U., Hoffmann, T., and Volkamer, R.: Effective Henry's law

partitioning and the salting constant of glyoxal in aerosols containing sulfate, Environ. Sci. Technol., 47, 4236-4244, 2013.

Kanaya, Y., Cao, R., Akimoto, H., Fukuda, M., Komazaki, Y., Yokouchi, Y., Koike, M., Tanimoto, H., Takegawa, N., and Kondo, Y.: Urban photochemistry in central Tokyo: 1. Observed and modeled OH and HO_2 radical concentrations during the winter and summer of 2004. J. Geophys. Res., 112(D21), https://doi.org/10.1029/2007JD008670, 2007.

Knote, C., Hodzic, A., Jimenez, J. L., Volkamer, R., Orlando, J. J., Baidar, S., Brioude, J., Fast, J., Gentner, D. R., and Goldstein, A. H.: Simulation of semi-explicit mechanisms of SOA formation from glyoxal in aerosol in a 3-D model, Atmos. Chem. Phys., 14, 6213-6239, 2014.

Li, X., Rohrer, F., Brauers, T., Hofzumahaus, A., and Wahner, A.: Modeling of HCHO and CHOCHO at a semi-rural site in southern China during the PRIDE-PRD2006 campaign, Atmos. Chem. Phys., 14, 33013-33054.

Lu, K. D., Rohrer, F., Holland, F., Fuchs, H., Bohn, B., Brauers, T., Chang, C.-C., Häseler, R., Hu, M., Kita, K., Kondo, Y., Li, X., Lou, S. R., Nehr, S., Shao, M., Zeng, L. M., Wahner, A., and Zhang, Y. H., Hofzumahaus, A.: Observation and modelling of OH and HO_2 concentrations in the Pearl River Delta 2006: a missing OH source in a VOC rich atmosphere, Atmos. Chem. Phys., 12, 1541-1569, 2012.

Ma, X., Tan, Z., Lu, K., Yang, X., Liu, Y., Li, S., Li, X., Chen, S., Novelli, A., Cho, C., and Zeng, L.: Winter photochemistry in Beijing: Observation and model simulation of OH and HO_2 radicals at an urban site, Sci. Total Environ., 685, 85-95, 2019.

Nan, J., Wang, S., Guo, Y., Xiang, Y., and Zhou, B.: Study on the daytime OH radical and implication for its relationship with fine particles over megacity of Shanghai, China, Atmos. Environ., 154, 167-178, 2017.

Pye, H. O. T., Murphy, B. N., Xu, L., Ng, N. L., Carlton, A. G., and Guo, H.: On the implications of aerosol liquid water and phase separation for organic aerosol mass, Atmos. Chem. Phys., 17, 343-369, 2017.

Ren, X., Brune, W. H., Mao, J., Mitchell, M. J., Lesher, R. L., Simpas, J. B., Metcalf, A. R., Schwab, J. J., Cai, C., Li, Y., and Demerjian, K. L.: Behavior of OH and HO_2 in the winter atmosphere in New York City, Atmos. Environ. 40, 252-263, 2006.

Tan, Z., Lu, K., Hofzumahaus, A., Fuchs, H., Bohn, B., Holland, F., Liu, Y., Rohrer, F., Shao, M., Sun, K. and Wu, Y.: Experimental budgets of OH, HO_2, and RO_2 radicals and implications for ozone formation in the Pearl River Delta in China 2014, Atmos. Chem. Phys., 19, 7129-7159, 2019.

Turpin, B. J., and Lim, H. J.: Species contributions to PM2.5 mass concentrations: Revisiting common assumptions for estimating organic mass, Aerosol Sci Technol., 35, 602-610, 2001.

Waxman, E. M., Elm, J., Kurtén, T., Mikkelsen, K. V., Ziemann, P. J., and Volkamer, R.: Glyoxal and methylglyoxal setschenow salting constants in sulfate, nitrate, and chloride solutions: Measurements and Gibbs energies, Environ. Sci. Technol., 49, 11500-11508.

Yuan, B., Hu, W. W., Shao, M., Wang, M., Chen, W. T., Lu, S. H., Zeng, L. M., and Hu, M.: VOC emissions, evolutions and contributions to SOA formation at a receptor site in eastern China, Atmos. Chem. Phys., 13, 8815-8832.